February, 2004

MODEL OF UNSTEADYn-OCTANEDROPLET BURNING INHIGH-TEMPERATURE STREAMS

Wei-Hsin Chen, *National Cheng Kung University*

Combust. Sci. and Tech., 176: 183–213, 2004

ISSN: 0010-2203 print/1563-521X online
DOI: 10.1080/00102200490255398

Taylor & Francis
Taylor & Francis Group

MODEL OF UNSTEADY *n*-OCTANE DROPLET BURNING IN HIGH-TEMPERATURE STREAMS

CHAO-CHUNG LIU

Department of Electrical Engineering,
Chung-Chou Institute of Technology, Yuan-lin, Changhua
Hsien, Taiwan, Republic of China

WEI-HSIN CHEN*

Department of Environmental Engineering and Sanitation,
Fooyin University, Taliao, Kaohsiung Hsien, Taiwan,
Republic of China

TSUNG LEO JIANG

Institute of Aeronautics and Astronautics, National Cheng
Kung University, Tainan, Taiwan, Republic of China

Unsteady burning, internal heating, and modeling comparison of an *n*-octane fuel droplet in high-temperature flows are studied numerically. In the developed numerical method, the governing equations of the gas and the liquid phases are fully solved and linked at the interface. In addition, a moving grid system and the particle deceleration are also considered to account for the droplet regression and impact of drag force. The obtained results show that the convective droplet is ignited with a wake flame after a heating-up period. With increasing time the relative velocity between the droplet and surrounding flow becomes smaller due to the drag. As a result, the flame changes from a wake type, through a transition type, and eventually to an envelope type. With regard to the droplet interior, internal heat transfer is always dominated by internal circulation and unsteady heating prevails over the entire droplet lifetime. The vaporization fluxes predicted in terms of

Received 15 October 2002; accepted 5 August 2003.
*Address correspondence to whchen@mail.fy.edu.tw

various quasi-steady models are also compared with the present solution. The quasi-steady analysis, omitting the initial droplet heat-up process, fails to predict the flame configurations and vaporization flux in the initial period of the droplet lifetime. Nevertheless, the role played by the initial unsteadiness on droplet vaporization is important only in a short period relative to the whole droplet lifetime. When the envelope flame develops around the droplet, the predictions by the quasi-steady models are in good agreement with the transient solution, except for the vaporization model. Furthermore, if the droplet undergoes a sudden drop in ambient temperature, it reveals that the dual solution of the quasi-steady model enables us to predict the droplet vaporization rate and flame configuration well.

Keywords: burning, droplet, vaporization, flame

INTRODUCTION

Rapid advances in computers and mathematical methods have greatly promoted numerical simulation as an analytical tool in solving various practical problems. However, its success is warranted only when the physical models embedded in the computer code are appropriate. This issue is of critical importance in spray combustion prediction. In the past, numerous outstanding investigations concerning droplet vaporization and combustion (Chiu, 2000; Dwyer, 1989; Faeth, 1977; Law, 1982, 1984; Sirignano, 1984) have been implemented to understand the fundamental characteristics of a droplet in sprays. In those studies, it was emphasized that the exchanges of mass, momentum, and energy between the gas phase and the droplet phase govern the reactive system. To predict the practical spray combustion by computation, droplet vaporization models could be established by analytical, numerical, or empirical formulas. The analytical formulas, in general, were conducted based on the studies of quasi-steady single-droplet vaporization and combustion in a stagnant environment or convective flow (Glassman, 1996; Kuo, 1986; Williams, 1985). With regard to the numerical and empirical formula, a number of correlations (Chiang, et al., 1992; Faeth and Lazar, 1971; Renksizbulut and Haywood, 1988) have been developed to aid modeling droplet gasification and motion. Upon inspection of the formulas and correlations, it is always presumed that only a unique value should be obtained, regardless of the historical state of the droplet.

In the earlier studies by Jiang et al. (1994, 1995), however, results indicate that multiple solutions of flame configuration and vaporization

rate may exist under certain flow conditions for a fuel droplet vaporizing in purely oxidizing or reactive flows. The flame configuration and the associated vaporization rate depend on the initially assumed state around the droplet and the process it undergoes. Specifically, when droplets initiate from different states and proceed through different processes to a state of the same ambient conditions, different flame configurations, such as envelope, transition, and wake flames, can exist at the same ambient Damköhler and Reynolds numbers. For instance, as a droplet is initially placed in a chemically frozen environment of low ambient temperature, it is expected to undergo the ignition process with increasing ambient Damköhler number. Alternatively, if an envelope flame at high ambient temperature initially surrounds a droplet, it will experience an extinction process with decreasing Damköhler number. As a result, corresponding to the low and the high initial energy constructions, a wake or transition flame in the former and an envelope flame in the latter can occur at the same Damköhler numbers. Because the droplet vaporization rate is highly related to the associated flame configuration, very different vaporization rates are expected even at the same ambient Damköhler number. The aforementioned characteristic is spoken of as a dual solution model. Basically, a similar result has also been observed by Chiu and Huang (1996; Huang and Chiu, 1997) in which the canonical droplet law was proposed to elucidate the interphase exchange rates. Furthermore, if droplet–droplet interaction in sprays is taken into consideration, because the leading droplet simultaneously acts as a fuel vapor source, a bluff-body, and an energy sink with respect to the trailing one (Chen, 2000a), this results in four different types of combustion hysteresis (Chen, 2000b; Chen et al., 1998) and multiple brachial burning (Chen, 2002) being induced. The cited literature clearly suggests that an appropriate evaluation of the droplet vaporization rate involves not only the instantaneous ambient conditions around the droplet but also the historical process that the droplet undergoes. It is thus apparent that the existing popularly adopted droplet vaporization models fail to account for such important multiple flame-configuration effects.

Aside from the multiple solutions, the other characteristic associated with the existing droplet vaporization models is the quasi-steady assumption in describing droplet vaporization and combustion. In the past, this assumption has been extensively applied in theoretical and experimental studies. The advantage of employing the quasi-steady assumption is that the transient effects during the droplet heat-up period

can be neglected, whereby it is not necessary to take the droplet internal heat transfer into account. Since Prakash and Sirignano (1978, 1980) employed the boundary-layer theory to study a vaporizing droplet, however, it has been recognized that the droplet internal heating is intrinsically unsteady (Sirignano, 1999). These transient effects might be significant in certain situations such as droplets in sprays that are primarily generated from a relatively cool region near the fuel nozzle. Under the foregoing situation the droplet temperature is initially lower than its wet-bulb point before entering the hot combustion zone. Hence, the droplet inevitably experiences the heat-up process during the early stage of its lifetime.

The preceding illustrations reveal that both multiple flame configurations and transient heating effects should be taken into account in modifying the existing droplet vaporization models, despite their popular usage in spray-combustion computation. However, it is known that as spray combustion is simulated, a huge amount of computational time is needed if the droplet internal heating is regarded. To provide a detailed observation concerning a convective droplet's combustion, the objective of the present study is to investigate the unsteady burning and internal heating of the droplet by means of fully solving the time-dependent Navier–Stokes equations of the gas and liquid phases. The preceding solution is referred to as the transient solution. The quasi-steady solutions in accordance with the studies of Faeth and Lazar (1971) and Jiang et al. (1994, 1995) will also be demonstrated to identify where and how the existing droplet vaporization models fail in estimating the droplet vaporization rate in spray-combustion computations. It will be elucidated that, with the exception of the initial heating period that occupies a small fraction of droplet lifetime, the dual solution model of Jiang et al. can provide a satisfactory prediction in droplet vaporization rate, whatever the ambient temperature changes.

FORMULATION

The physical configuration of this study is sketched in Figure 1. Instead of describing the droplet moving through the gas, the reference frame from a stationary environment is changed to a system with moving gas by using an Eulerian formulation to facilitate the computation. In other words, the fixed origin of the axisymmetric coordinate is located at the

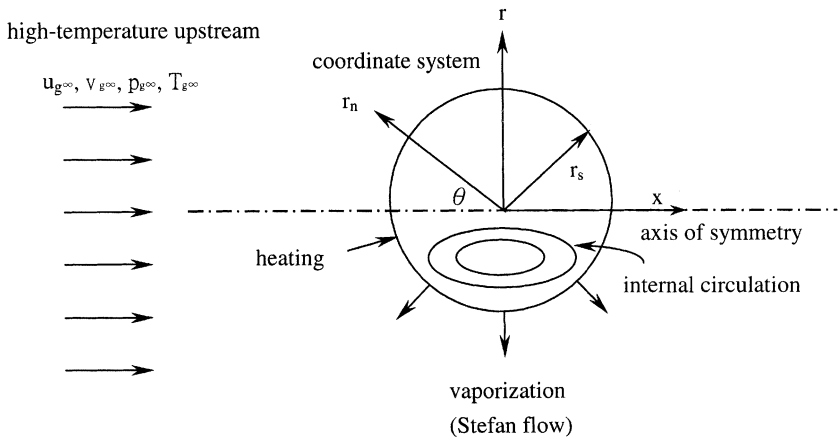

Figure 1. Schematic diagram of used coordinate systems and illustration of a vaporizing droplet in flow.

center of the droplet. It represents an axisymmetric, high-temperature convective flow over a fuel droplet in an environment of atmospheric pressure. For a droplet in sprays, when the body force is considered, it has been elucidated (Sirignano, 1984) that the effect of buoyant force is negligible because of small Grashof number. Specifically, when a droplet's radius is 100 μm while the environmental pressure is atmospheric, the order of the Grashof number is about $O(10^{-2})$, much smaller than one. Therefore, the body force is disregarded. Effects of thermal radiation and droplet deformation are also neglected on account of secondary importance at low pressure. Fick's law is assumed for the species diffusion velocity. Gas-phase combustion is approximated by single-step global finite rate chemical reaction (Chen, 2000a). Variations in specific heat, viscosity, diffusion coefficient, and thermal conductivity over temperature have been taken into account through appropriate kinetic-theory models or correlations (Reid et al., 1988). The specific heat of the gas mixture is evaluated from the ideal gas mixing rule. The governing equations of the gas phase include the continuity, momentum, energy, and species conservation equations, as well as the equation of state. The liquid phase consists of the same governing equations, excluding the species equation and equation of state. The governing equations for both phases are given as follows.

Gas Phase

Continuity equation:

$$\frac{\partial \rho_g}{\partial t} + \frac{\partial}{\partial x}(\rho_g u_g) + \frac{1}{r}\frac{\partial}{\partial r}(r\rho_g v_g) = 0 \tag{1}$$

Axial momentum equation:

$$\begin{aligned}\frac{\partial}{\partial t}(\rho_g u_g) + \frac{\partial}{\partial x}\left(\rho_g u_g u_g - \mu_g \frac{\partial u_g}{\partial x}\right) + \frac{1}{r}\frac{\partial}{\partial r}\left(r\rho_g u_g v_g - r\mu_g \frac{\partial u_g}{\partial r}\right) \\ = -\frac{\partial p_g}{\partial x} + \frac{\partial}{\partial x}\left\{-\frac{2}{3}\mu_g\left[\frac{\partial u_g}{\partial x} + \frac{1}{r}\frac{\partial}{\partial r}(r v_g)\right] + \mu_g \frac{\partial u_g}{\partial x}\right\} \\ + \frac{1}{r}\frac{\partial}{\partial r}\left(r\mu_g \frac{\partial v_g}{\partial x}\right)\end{aligned} \tag{2}$$

Radial momentum equation:

$$\begin{aligned}\frac{\partial}{\partial t}(\rho_g v_g) + \frac{\partial}{\partial x}\left(\rho_g u_g v_g - \mu_g \frac{\partial v_g}{\partial x}\right) + \frac{1}{r}\frac{\partial}{\partial r}\left(r\rho_g v_g v_g - r\mu_g \frac{\partial v_g}{\partial r}\right) \\ = -\frac{\partial p_g}{\partial r} + \frac{1}{r}\frac{\partial}{\partial r}\left\{r\mu_g \frac{\partial v_g}{\partial x} - \frac{2}{3}r\mu_g\left[\frac{\partial u_g}{\partial x} + \frac{1}{r}\frac{\partial}{\partial r}(r v_g)\right]\right\} \\ + \frac{\partial}{\partial x}\left(\mu_g \frac{\partial u_g}{\partial r}\right) - 2\mu_g \frac{v_g}{r^2} + \frac{2}{3}\frac{\mu_g}{r}\left(\frac{\partial u_g}{\partial x} + \frac{1}{r}\frac{\partial}{\partial r}(r v_g)\right)\end{aligned} \tag{3}$$

Energy equation:

$$\begin{aligned}\frac{\partial}{\partial t}(\rho_g h_g) + \frac{\partial}{\partial x}\left(\rho_g u_g h_g - k_g \frac{\partial T_g}{\partial x}\right) + \frac{1}{r}\frac{\partial}{\partial r}\left(r\rho_g v_g h_g - r k_g \frac{\partial T_g}{\partial r}\right) \\ = Q\dot{\omega} + \mu_g\left\{2\left[\left(\frac{\partial u_g}{\partial x}\right)^2 + \left(\frac{\partial v_g}{\partial r}\right)^2 + \left(\frac{v_g}{r}\right)^2\right] + \left(\frac{\partial u_g}{\partial r} + \frac{\partial v_g}{\partial x}\right)^2\right\}\end{aligned} \tag{4}$$

where

$$h = \sum_{i=1}^{N} Y_i \int_{298K}^{T} C_{p,i}\, dT \tag{5}$$

Species conservation equations:

$$\frac{\partial}{\partial t}(\rho_g Y_i) + \frac{\partial}{\partial x}\left(\rho_g u_g Y_i - \rho_g D_g \frac{\partial Y_i}{\partial x}\right) + \frac{1}{r}\frac{\partial}{\partial r}\left(r\rho_g v_g Y_i - r\rho_g D_g \frac{\partial Y_i}{\partial r}\right) = -\nu_i W_i \dot{\omega} \tag{6}$$

Equation of state:

$$p_g = \rho_g R_u T_g \sum_{i=1}^{N} \frac{Y_i}{W_i} \tag{7}$$

Gas-phase combustion (Westbrook and Dryer, 1981):

$$\dot{\omega} = A \exp\left(-\frac{E_a}{RT}\right)[C_8H_{18}]^{0.25}[O_2]^{1.5} \tag{8}$$

In the foregoing equation, $A\,(=4.6\times10^{11})$ and $E_a(=30\,\text{Kcal/mol})$ are preexponential factor and activation energy, respectively.

Liquid Phase

Continuity equation:

$$\frac{\partial \rho_l}{\partial t} + \frac{\partial}{\partial x}(\rho_l u_l) + \frac{1}{r}\frac{\partial}{\partial r}(r\rho_l v_l) = 0 \tag{9}$$

Axial momentum equation:

$$\frac{\partial}{\partial t}(\rho_l u_l) + \frac{\partial}{\partial x}\left(\rho_l u_l u_l - \mu_l \frac{\partial u_l}{\partial x}\right) + \frac{1}{r}\frac{\partial}{\partial r}\left(r\rho_l u_l v_l - r\mu_l \frac{\partial u_l}{\partial r}\right) = -\frac{\partial p_l}{\partial x} + \frac{\partial}{\partial x}\left\{-\frac{2}{3}\mu_l\left[\frac{\partial u_l}{\partial x} + \frac{1}{r}\frac{\partial}{\partial r}(r v_l)\right] + \mu_l \frac{\partial u_l}{\partial x}\right\} + \frac{1}{r}\frac{\partial}{\partial r}\left(r\mu_l \frac{\partial v_l}{\partial x}\right) \tag{10}$$

Radial momentum equation:

$$\frac{\partial}{\partial t}(\rho_l v_l)+\frac{\partial}{\partial x}\left(\rho_l u_l v_l-\mu_l\frac{\partial v_l}{\partial x}\right)+\frac{1}{r}\frac{\partial}{\partial r}\left(r\rho_l v_l v_l-r\mu_l\frac{\partial v_l}{\partial r}\right)$$
$$=-\frac{\partial p_l}{\partial r}+\frac{1}{r}\frac{\partial}{\partial r}\left\{r\mu_l\frac{\partial v_l}{\partial x}-\frac{2}{3}r\mu_l\left[\frac{\partial u_l}{\partial x}+\frac{1}{r}\frac{\partial}{\partial r}(rv_l)\right]\right\}+\frac{\partial}{\partial x}\left(\mu_l\frac{\partial u_l}{\partial r}\right)$$
$$-2\mu_l\frac{v_l}{r^2}+\frac{2}{3}\frac{\mu_l}{r}\left(\frac{\partial u_l}{\partial x}+\frac{1}{r}\frac{\partial}{\partial r}(rv_l)\right) \tag{11}$$

Energy equations:

$$\frac{\partial}{\partial t}(\rho_l h_l)+\frac{\partial}{\partial x}\left(\rho_l u_l h_l-k_l\frac{\partial T_l}{\partial x}\right)+\frac{1}{r}\frac{\partial}{\partial r}\left(r\rho_l v_l h_l-rk_l\frac{\partial T_l}{\partial r}\right)$$
$$=\mu_l\left\{2\left[\left(\frac{\partial u_l}{\partial x}\right)^2+\left(\frac{\partial v_l}{\partial r}\right)^2+\left(\frac{v_l}{r}\right)^2\right]+\left(\frac{\partial u_l}{\partial r}+\frac{\partial v_l}{\partial x}\right)^2\right\} \tag{12}$$

The initial conditions corresponding to the sudden injection of a cold droplet into a uniform flow are as follows for the gas phase,

$$\begin{aligned} &u_g=u_{g\infty}\quad v_g=0\quad p_g=p_{g\infty}\\ &T_g=T_{g\infty}\quad \rho_g=\rho_{g\infty}\quad Y_f=0\end{aligned} \tag{13}$$

and for the liquid phase,

$$u_l=v_l=0\quad T_l=T_{l0}\quad \rho_l=\rho_{l0} \tag{14}$$

To provide a clear description of the boundary conditions, they are expressed in terms of spherical coordinates (r_n, θ) rather than the cylindrical coordinate with axisymmetry, as shown in Figure 1. Though the coordinate system of the boundary conditions is different from that of the governing equations, the given boundary conditions have already been transformed into the axisymmetric coordinate during calculation. The boundary conditions are given as follows.
Upstream inflow ($r_n=r_\infty$, $0\le\theta\le\pi/2$):

$$u_g=u_{g\infty}\quad v_g=0\quad p_g=p_{g\infty}\quad T_g=T_{g\infty}\quad Y_f=0 \tag{15}$$

Downstream outflow ($r_n = r_\infty$, $\pi/2 < \theta \leq \pi$):

$$\frac{Du_g}{Dt} = \frac{Dv_g}{Dt} = \frac{Dp_g}{Dt} = \frac{DT_g}{Dt} = \frac{DY_f}{Dt} = 0 \tag{16}$$

Axis of symmetry ($0 \leq r_n \leq r_\infty$, $\theta = 0$ or $\theta = \pi$):

$$v_g = \frac{\partial u_g}{\partial \theta} = \frac{\partial p_g}{\partial \theta} = \frac{\partial T_g}{\partial \theta} = \frac{\partial Y_f}{\partial \theta} = 0 \tag{17}$$

$$v_l = \frac{\partial u_l}{\partial \theta} = \frac{\partial p_l}{\partial \theta} = \frac{\partial T_l}{\partial \theta} = 0 \tag{18}$$

Gas–liquid interface ($r_n = r_s$, $0 \leq \theta \leq \pi$):

$$v_{g\theta} = v_{l\theta} \tag{19}$$

$$T_g = T_l \tag{20}$$

$$\mu_g \left(\frac{\partial v_\theta}{\partial r_n} - \frac{v_\theta}{r_s} + \frac{1}{r_s} \frac{\partial v_n}{\partial \theta} \right)_g = \mu_l \left(\frac{\partial v_\theta}{\partial r_n} - \frac{v_\theta}{r_s} + \frac{1}{r_s} \frac{\partial v_n}{\partial \theta} \right)_l \tag{21}$$

$$\dot{m}_\theta = \dot{m}_\theta Y_f - \rho_g D_g \left(\frac{\partial Y_f}{\partial r_n} \right) \tag{22}$$

$$\dot{m}_\theta L = k_g \left(\frac{\partial T}{\partial r_n} \right)_g - k_l \left(\frac{\partial T}{\partial r_n} \right)_l \tag{23}$$

$$\rho_g v_{gn} - \rho_g \frac{dr_s}{dt} = \rho_l v_{ln} - \rho_l \frac{dr_s}{dt} = \dot{m}_\theta \tag{24}$$

$$\ln \left(\frac{p_{fs}}{p_{ref}} \right) = \frac{L}{R_u} \left(\frac{1}{T_{ref}} - \frac{1}{T_s} \right) \tag{25}$$

Because the phase equilibrium is assumed to prevail at the interface, the Clausius–Clapeyron relation, Eq. (25), is employed to relate fuel vapor pressure and the droplet surface temperature. After a droplet is injected from the nozzle, the relative velocity between the droplet and the gas-phase flow progressively decreases with time as a consequence of the drag. On the other hand, as mentioned earlier, because the reference

frame is fixed to the droplet, a reversed D'Alembert force due to the drag force on the droplet is applied to the gas-phase flow field. The total drag is composed of three components, including pressure drag, friction drag, and thrust drag (Chiang et al., 1992). The drag coefficients are expressed as follows.

Pressure drag coefficient:

$$C_{\mathrm{Dp}} = \frac{2}{\rho_{\mathrm{g}\infty} u_{\mathrm{g}\infty}^2} \int_0^{\pi} (p_{\mathrm{s}} - p_{\infty}) \sin 2\theta \, d\theta \tag{26}$$

Friction drag coefficient:

$$C_{\mathrm{Df}} = \frac{4}{\rho_{\mathrm{g}\infty} u_{\mathrm{g}\infty}^2} \int_0^{\pi} \mu_{\mathrm{g}} \left(\frac{\partial v_{\mathrm{g}\theta}}{\partial r} - \frac{v_{\mathrm{g}\theta}}{r} + \frac{1}{r} \frac{\partial v_{\mathrm{gn}}}{\partial \theta} \right) \sin^2 \theta \, d\theta$$
$$- \frac{4}{3\rho_{\mathrm{g}\infty} u_{\mathrm{g}\infty}^2} \int_0^{\pi} \mu_{\mathrm{g}} \left(2 \frac{\partial v_{\mathrm{gn}}}{\partial r} - 2 \frac{v_{\mathrm{gn}}}{r} - \frac{1}{r} \frac{\partial v_{\mathrm{g}\theta}}{\partial \theta} - \frac{v_{\mathrm{gn}}}{r} \frac{\cos\theta}{\sin\theta} \right) \sin 2\theta \, d\theta \tag{27}$$

Thrust drag coefficient:

$$C_{\mathrm{Dt}} = \frac{2}{\rho_{\mathrm{g}\infty} u_{\mathrm{g}\infty}^2} \int_0^{\pi} \left[\rho_{\mathrm{g}} v_{\mathrm{gn}} \left(v_{\mathrm{gn}} \sin\theta - 2 v_{\mathrm{g}\theta} \sin^2 \theta \right) \right] d\theta \tag{28}$$

Total drag coefficient:

$$C_{\mathrm{D}} = C_{\mathrm{Dp}} + C_{\mathrm{Df}} + C_{\mathrm{Dt}} \tag{29}$$

Accordingly, the droplet deceleration is determined from the preceding equation and it is expressed as

$$\frac{du_{\mathrm{d}}}{dt} = -\frac{3}{8} \frac{\rho_{\mathrm{g}\infty}}{\rho_{\mathrm{l}}} \frac{u_{\mathrm{g}\infty}^2}{r_0} C_{\mathrm{D}} \tag{30}$$

The decrement in the relative velocity between the freestream and the droplet within a short time Δt is calculated by

$$\Delta u = \Delta t \times \frac{du_{\mathrm{d}}}{dt} \tag{31}$$

The far-field velocity is thus adjusted by

$$u_{g\infty}(x, r, t + \Delta t) = u_{g\infty}(x, r, t) + \Delta u \tag{32}$$

NUMERICAL METHOD

Upon inspection of the governing equations of the physical problem, it is recognized that finding the analytical solutions of the equations is impossible due to their nonlinearity and coupling. Instead, one has to develop a numerical method to simulate the physical phenomena. In the present study, the governing equations of both the gas and liquid phases are fully solved through the numerical method. In this method, the equations are first discretized into their algebraic counterparts based on the finite-volume method (Patankar, 1980). Then, the SIMPLER algorithm in conjunction with iterative procedure is applied to solve the two-phase flow fields. As a whole, the entire computational domain is divided into two different regions (i.e., the gas phase and the liquid phase). The gas-phase equations are solved first and then the obtained interfacial variables become the boundary conditions of the liquid phase. Subsequently, the liquid-phase equations are calculated. Because a number of interfacial conditions are involved when solving the two-phase equations, the Newton–Raphson scheme is utilized to accelerate the convergence. The foregoing procedure is reiterated until the interfacial conditions and required convergent criteria are satisfied. During the calculation, the line-by-line TriDiagonal-Matrix Algorithm is used as an equation solver, while the block correction procedure (Patankar, 1981) is incorporated in the numerical method for increasing the computational efficiency. In the meantime, the power-law scheme is used for the convective and diffusive fluxes over the control volume surface.

To reduce the numerical truncation errors stemming from the nonuniform grids, the grid locations along the normal direction of the interface are distributed by use of the hyperbolic tangent function (Thomposon et al., 1985). By virtue of severe variations of the scalar variables, such as temperature and fuel concentration, near the droplet surface, the grid distribution is controlled to be finer nearby. The grid system consists of 75×41 grids for the gas-phase flow and 25×41 grids for the liquid-phase flow. Twenty times of droplet radius on the investigated domain are selected. In the study by Jiang et al. (1994), a

variety of grid systems and computational domains have been tested and compared with each other. As a result, it was verified that the earlier-specified computation domain is far enough for investigating a burning droplet. Moreover, it was also illustrated that the presently adopted grid system can provide a satisfactory requirement on grid independence. The grid distributions of both the gas and liquid phases are displayed in Figure 2. The fully implicit scheme is utilized for time marching calculation. When a fuel droplet is immersed in a high-temperature flow, it is known that the droplet will be vaporized so it shrinks with increasing time. That is to say, the interfacial grid position changes continuously with time. In order to overcome this numerical difficulty, a moving grid system (Thompson et al., 1985) is introduced in the developed code. On the other hand, the relative velocity between the gas-phase flow and the droplet gradually decreases with time due to the drag. Hence, the drag is calculated to modify the relative velocity between the two phases. The global transport behavior has been illustrated from Eqs. (26)–(32). To ensure the validation of the present computer code, time variations of the three drag coefficients of an evaporating fuel droplet are performed and compared with the result of Chiang et al. (1992). Figure 3 depicts that the present result is quite consistent with the published results.

RESULTS AND DISCUSSION

Attention of this study is placed on the burning of an *n*-octane (n-C_8H_{18}) droplet in flow. The initial temperatures of the droplet and the ambience are set as 300 and 1000 K, respectively. Meanwhile, the initial relative velocity between the droplet and the freestream is 40 m/s and the initial droplet radius is 100 μm. Under this condition, the initial droplet Reynolds number ($\mathrm{Re}_0 = 2\rho_{g\infty}u_{g\infty}r_0/\mu_{g\infty}$) is approximately 70. In the following discussion, gas-phase burning process and transient internal heating of the droplet, as well as droplet modeling, will be illustrated sequentially in terms of the convective time (viz. $t' = 2r_{s,0}/u_{g\infty,0} = 5\times 10^{-6}$ s).

Gas-Phase Burning Process

Figures 4 and 5 show the temporal mass fraction and isothermal patterns, respectively, in which the concentration and temperature contours are

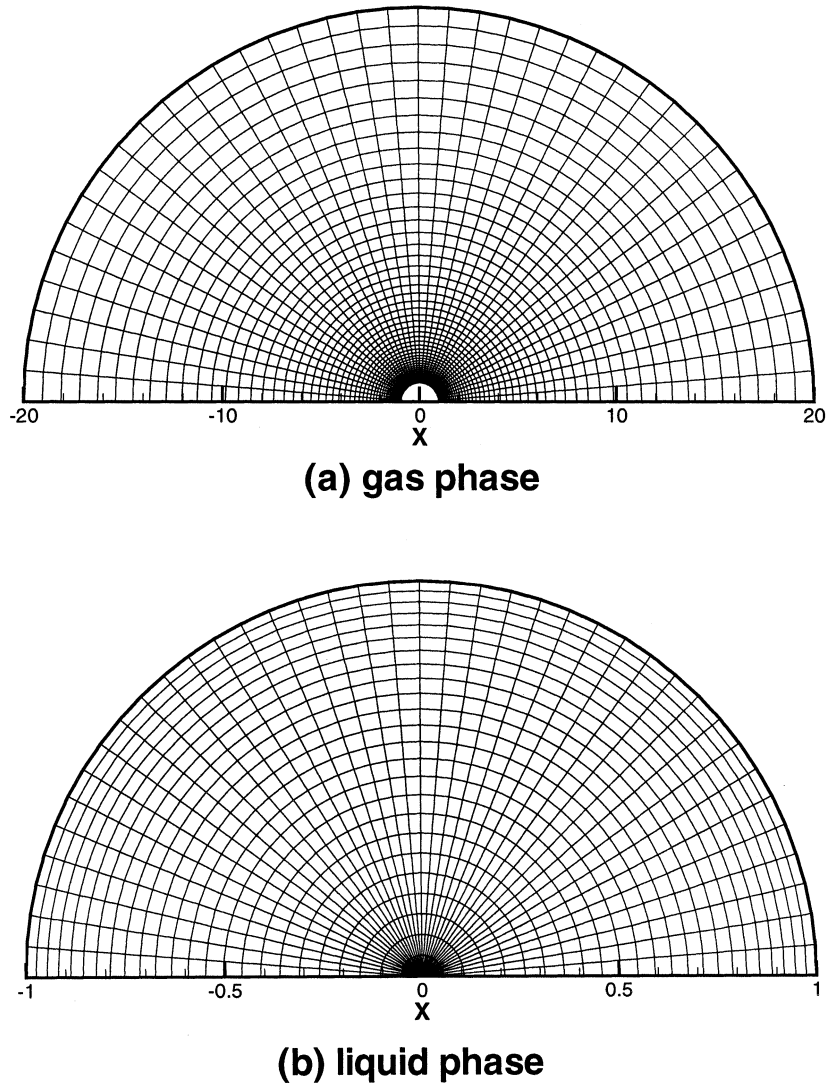

Figure 2. Grid distributions of (*a*) gas phase and (*b*) liquid phase.

represented by grayscales. Once a droplet is injected into a hot environment, heat transfer between the two phases begins resulting from the temperature gradient in the vicinity of the interface. In the early stage, most of the heat transferred from the ambience to the droplet is used to

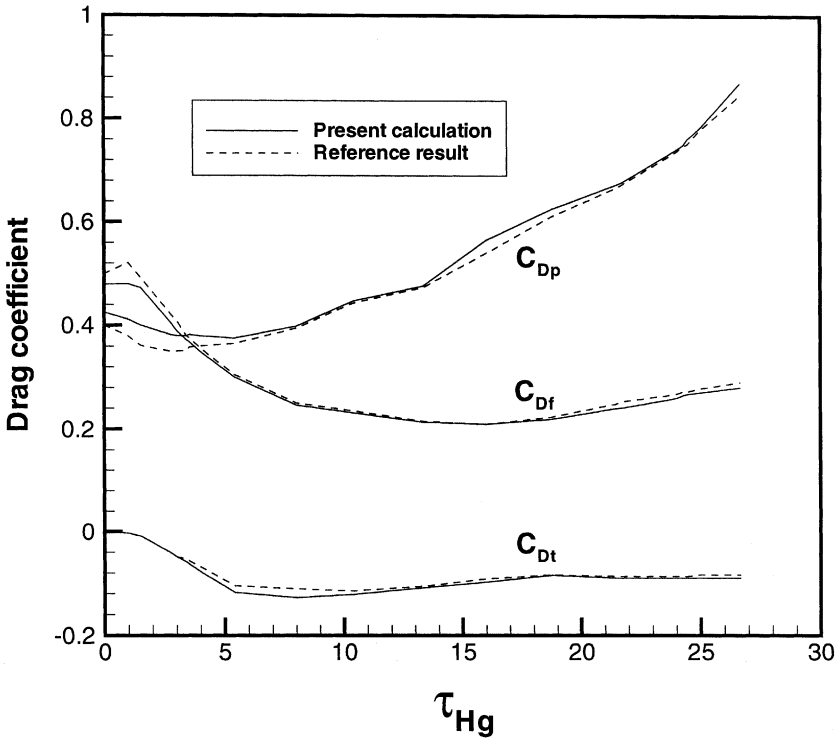

Figure 3. Comparisons of predicted drag coefficients of an evaporating fuel droplet with respect to time.

heat up the droplet; only a small fraction of the heat is used to vaporize the fuel droplet (Figure 4*a*). Therefore, it can be seen that, at $5t'$, the chemical reaction around the droplet is so weak that the gaseous maximum temperature is almost imperceptible (Figure 5*a*) relative to the surrounding temperature. Increasing time increases the fuel vapor amount and it is brought to the wake region of the droplet (Figure 4*b*). Basically, the droplet plays a role of bluff-body; that is, the flow behind the droplet is retarded and the fuel vapor is accumulated therein. This provides an environment where the fuel and the oxidizer are premixed, which is conducive to combustion; hence, at $200t'$ a wake flame is observed in the downstream region of the droplet (Figure 5*b*). Thereafter, because more fuel is vaporized from the droplet (Figure 4*c*) and the energy generated from chemical reaction is increased as well, when the

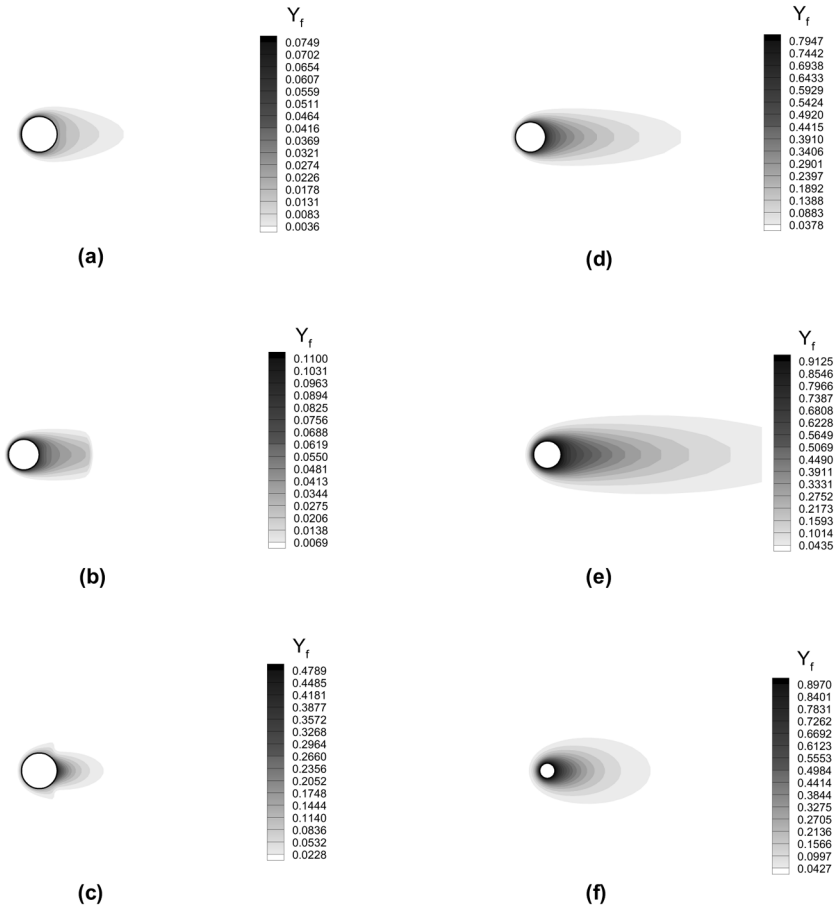

Figure 4. Fuel concentration contours in the gas phase at (*a*) $5t'$, (*b*) $200t'$, (*c*) $500t'$, (*d*) $1300t'$, (*e*) $4000t'$, and (*f*) $8000t'$.

time is $500t'$ the wake flame propagates upstream, which is very close to the droplet (Figure 5*c*). With increasing time, the relative velocity between the droplet and the ambience decreases due to the drag. Besides, the droplet shrinks as a consequence of vaporization. These two factors make the Reynolds number in terms of the relative velocity and droplet diameter decrease, as shown in Figure 6 where the distributions of droplet size and Reynolds number with respect to time are demonstrated. Accordingly, at $1300t'$ the flame moves farther forward against the flow, thereby yielding a transition flame (Figure 5*d*). As the flame moves closer

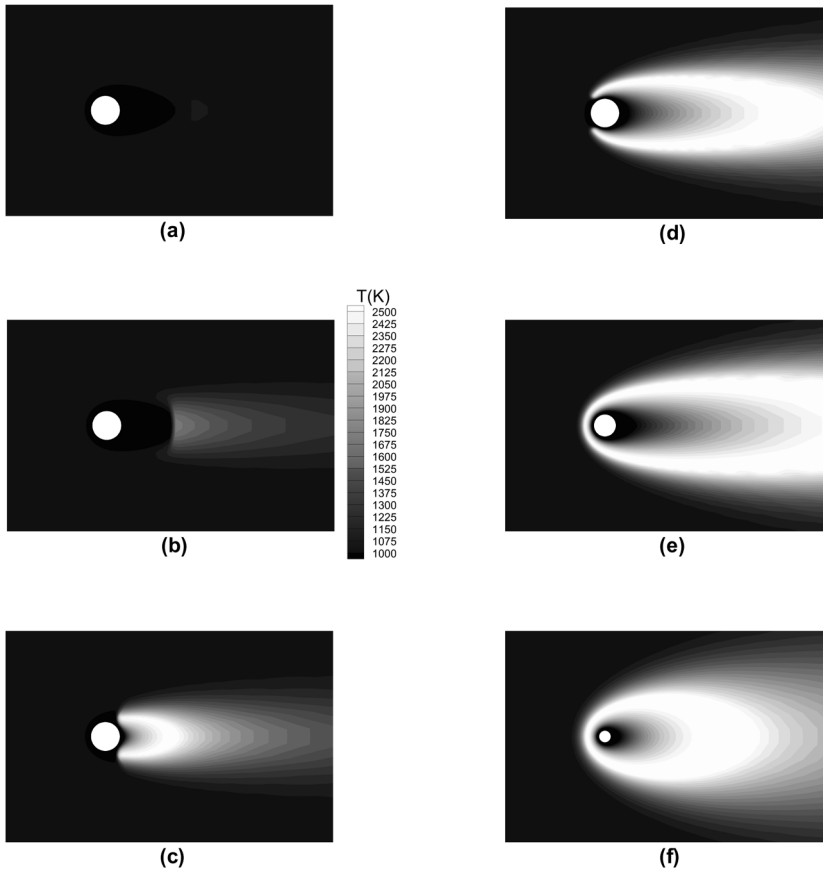

Figure 5. Isothermal contours in the gas phase at (*a*) $5t'$, (*b*) $200t'$, (*c*) $500t'$, (*d*) $1300t'$, (*e*) $4000t'$, and (*f*) $8000t'$.

to the droplet, more fuel vapor is released (Figure 4*d*). This obviously enhances the chemical reaction and increases the flame speed, rendering the flame moving farther toward the droplet. When the time is $4000t'$, an envelope flame surrounding the droplet is clearly observed (Figure 5*e*), and the droplet becomes quite small at $8000t'$ (Figure 5*f*). Specifically, at this specific time 85% of the droplet mass has already been vaporized, as shown in Figure 6. As a whole, the flame evolves from a wake type to a side type, and then into an envelope type. In the study by Chiu and Hu (1998), a concept of scavenging combustion was proposed to describe the

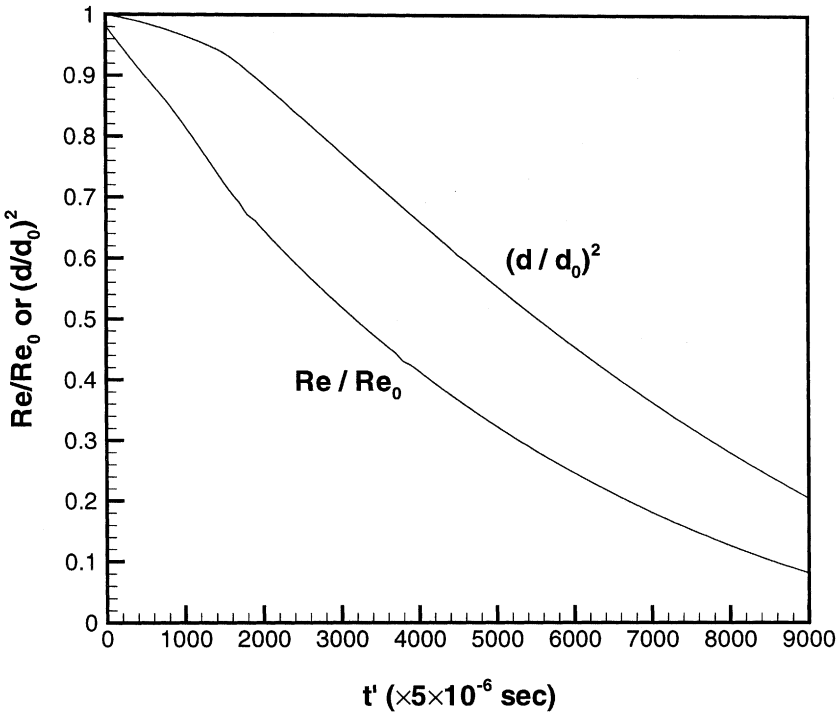

Figure 6. Distributions of droplet size and Reynolds number with respect to time.

role of fuel vapor sink played by flame. In contrast to the present result, when the flame moves upstream and approaches the droplet, the fuel vapor contour ahead of the flame is apparently skewed as a result of depletion (Figure 4*c*). When the flame encompasses the droplet, the fuel vapor is always enclosed inside the flame, whereas the oxidizer is isolated outside the flame. Under such a situation, the droplet combustion converts the premixed flame (i.e., the wake and transition flames) to the diffusion flame (i.e., the envelope flame).

Internal Heating of the Convective Droplet

Subsequently, the droplet internal streamlines and isothermal contours at various times are demonstrated in Figures 7 and 8, respectively. Figure 7*a* depicts that soon after the droplet is immersed in a convective

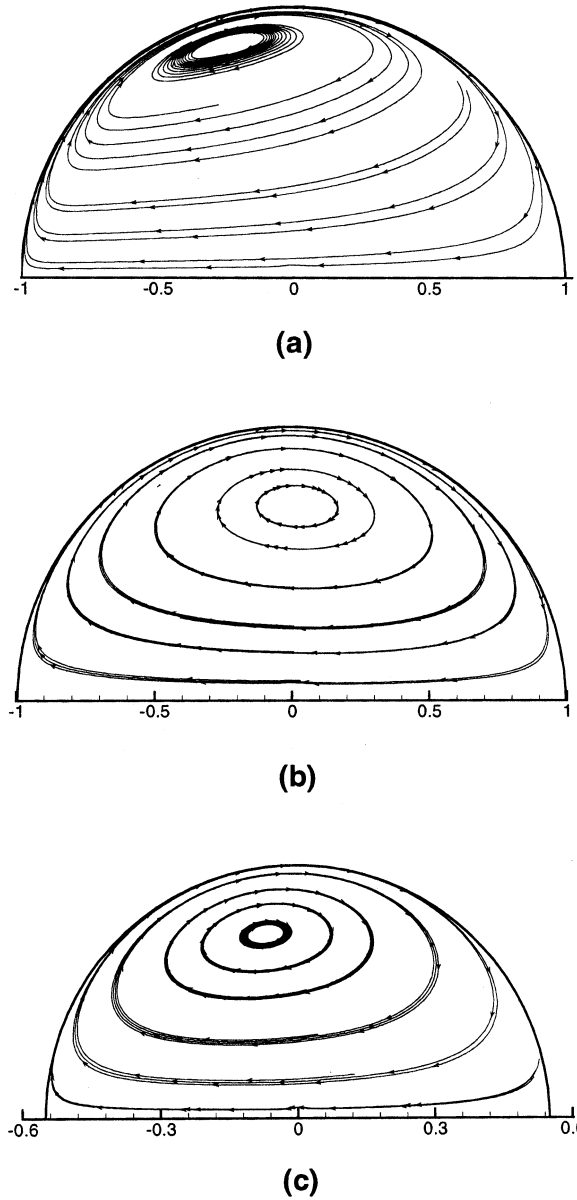

Figure 7. Streamline distributions in the droplet at (*a*) $5t'$, (*b*) $500t'$, and (*c*) $8000t'$.

flow, at $5t'$ the vortex motion develops in the droplet interior. Nevertheless, in view of the concentration of the streamlines and the vortex core near the droplet surface, it is recognized that the early momentum transfer mainly occurs adjacent to the interface. In the meantime, the isothermal pattern (Figure 8*a*) shows that the majority of heat transferred from the gas phase is accumulated in the region very close to the droplet surface. Then, at $200t'$ most of the heat absorbed by the droplet is transported to the aft region inside the droplet (Figure 8*b*). This arises from the fact that, following heat diffused from the interface, the energy is rapidly brought away by streamlines. When the time is $500t'$, the vortex core is approximately located at two-third radius away from the

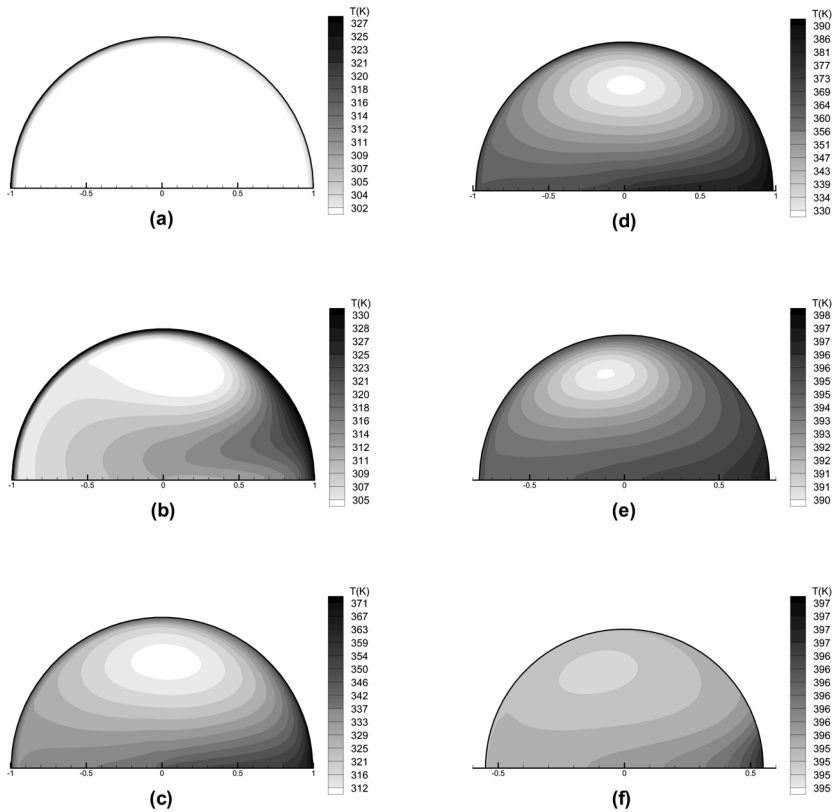

Figure 8. Isothermal contours in the droplet at (*a*) $5t'$, (*b*) $200t'$, (*c*) $500t'$, (*d*) $1300t'$, (*e*) $4000t'$, and (*f*) $8000t'$.

droplet center (Figure 7*b*) and it almost develops fully at $8000t'$ (Figure 7*c*). Basically, when the time is long enough (say, time $\geq 500t'$), the temperature distributions in the droplet interior (Figures 8*c–f*) resemble the streamline distributions. Specifically, the vortex center always remains at the minimum temperature, whereas the maximum temperature point is located near the aft stagnation point. This reveals that the heat transfer in the droplet interior is dominated by internal recirculation. In other words, the energy is transported across the streamlines toward the vortex center. It is also noted that when the time is $4000t'$ the internal temperature distribution becomes uniform to a certain extent (Figure 8*e*). In fact, if a droplet is immersed in a flow in the absence of evaporation, the transient period for fluid to form a steady internal vortex can be roughly estimated as follows (Prakash and Sirignano, 1978):

$$\tau_{\text{vortex formation}} = O\left(\frac{r_s^2}{\nu_l}\right) \tag{33}$$

where ν_l is the kinematic viscosity of the fuel. Considering the heat transfer in the droplet with strong motion, the characteristic time of heat diffusion can be represented by (Prakash and Sirignano, 1978; Wong and Lin, 1992)

$$\tau_{\text{heat diffusion}} = O\left(\frac{(0.3r_s)^2}{\alpha_l}\right) \tag{34}$$

Dividing Eq. (34) by Eq. (33) gives

$$\frac{\tau_{\text{heat diffusion}}}{\tau_{\text{vortex formation}}} = O\left(\frac{\frac{(0.3r_s)^2}{\alpha_l}}{\frac{r_s^2}{\nu_l}}\right) = O\left(0.09\frac{\nu_l}{\alpha_l}\right) = O(0.09Pr_l) \approx 7.35 \text{ at } 398.81^\circ\text{C} \tag{35}$$

Since the value of Eq. (35) is larger than unity, the vortex formation is established earlier than heat diffusion as observed. It should be mentioned that the Stefan flow induced from droplet heating complicates the physical problem; hence, the preceding analysis just provides a fundamental insight into the droplet internal transport processes.

Time variations of droplet vaporization flux with and without chemical reaction are presented in Figure 9, in which the temporal evolution of flame configuration is displayed as well. Clearly, for the burning droplet, the vaporization flux increases monotonically with time as the flame configuration evolves from pure vaporization, through a wake flame, a transition flame, and then to an envelope flame. Moreover, the figure suggests that the envelope flame occupies most of the period of droplet burning. It is noteworthy that the vaporization flux increases significantly in the course of the transition flame becoming an envelope flame. In regard to the evaporating droplet (i.e., without chemical reaction), it can be seen that its mass flux is identical to that of the burning droplet before the transition flame is formed. Thereafter, the mass flux of the former is much smaller than that of the latter. Considering an evaporating droplet (Sirignano, 1984), it has been illustrated that the mass transfer along the interface is mainly contributed from the

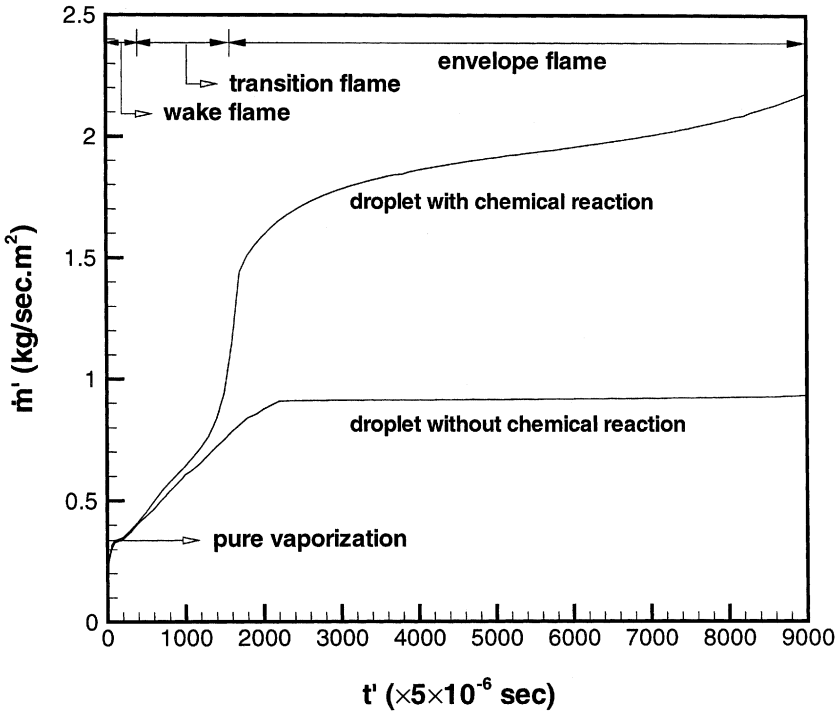

Figure 9. Distribution of droplet vaporization flux with respect to time (transient solution).

front portion of the droplet. In contrast, for a burning droplet, as long as the flame approaches or reaches the front stagnation point of the droplet (about $1500t'$), the mass transfer rate will be intensified profoundly. The preceding observation clearly reflects that the vaporization rate is deeply related to the flame configuration.

Modeling Comparison of the Convective Droplet

Based on the present study, the limitations of two selected quasi-steady models applied to aid prediction of spray combustion will be assessed. The first one is the empirical correlation conducted by Faeth and Lazar (1971). In their formula, the vaporization rate for a droplet in a convective flow, relative to a stationary environment, is correlated by

$$\frac{\dot{m}}{\dot{m}_0} = 1 + \frac{0.278\ Re^{1/2} Sc^{1/3}}{1 + \frac{1.232}{(Re\ Sc^{4/3})^{1/2}}} \tag{36}$$

According to the classical droplet theory, the stationary droplet vaporization rate is given by

$$\dot{m}_0 = 4\pi r_s \rho_s D_s \ln(1 + B) \tag{37}$$

where B is the Spalding transfer number (Kuo, 1986). The preceding model can be utilized for both cases of droplet vaporization and combustion. However, an ignition criterion has to be employed to determine the droplet burning status before the vaporization or combustion model is chosen. The second one is the dual solution model proposed by Jiang et al. (1994, 1995). Their model includes the lower- and upper-branch solutions corresponding to an initially nonburning droplet and a burning droplet, respectively. The detailed profiles of droplet vaporization flux in accordance with the various models and the transient solutions are demonstrated in Figure 10. In the early period of the droplet lifetime, all the quasi-steady models fail when predicting the droplet vaporization flux. This result is not surprising since the quasi-steady models do not take the droplet internal heating into account; hence, they overestimate the vaporization fluxes. By comparing all of the quasi-steady models, when an envelope flame occurs, the vaporization model of Faeth and Lazar substantially underestimates the droplet vaporization flux.

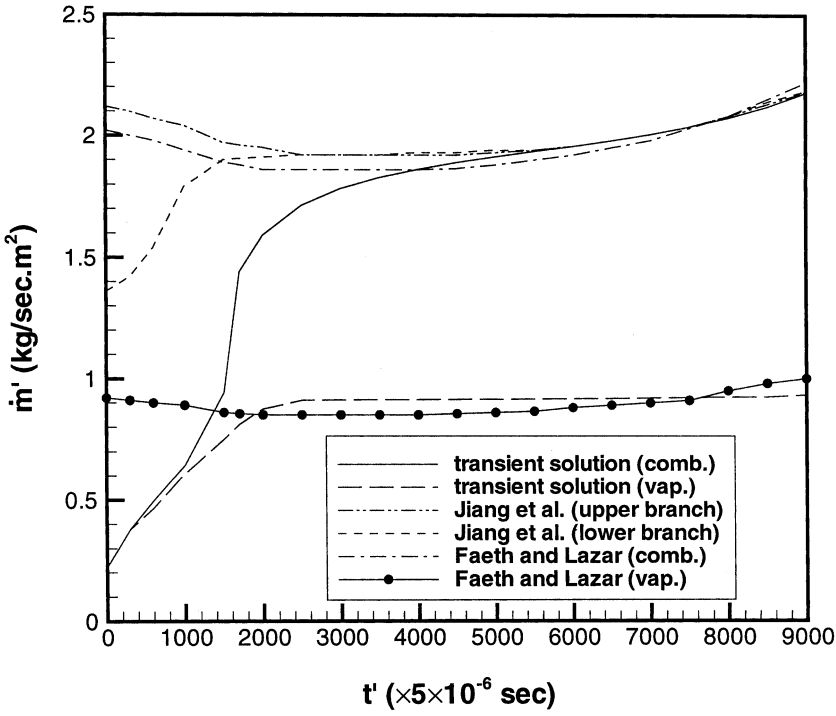

Figure 10. Comparison of droplet vaporization fluxes with respect to time.

The lower-branch solution of Jiang et al. offers the best match in trend with the present transient solution. However, without considering the droplet heat-up process, the lower-branch solution tends to release more fuel vapor initially and to ignite the droplet at an earlier instant. As a result, the envelope flame appears earlier and the vaporization flux is overpredicted. Compared with the lower-branch solution, the predictions by the upper-branch solution of Jiang et al. and the combustion model of Faeth and Lazar depart more from the transient solution, a consequence of the presumption of an initially burning droplet in both solutions. It should be mentioned that despite their poor agreement with the transient solution in the initial period, once an envelope flame encloses the fuel droplet, the predictions by the quasi-steady models, except for the vaporization model of Faeth and Lazar, agree well with the present result. This is attributed to the fact that the temperature gradient in the droplet tends to decrease, rendering the internal heating effects minimal.

The transient effects are also important when the ambient temperature experiences a sudden change. Two cases are taken into account. In the first case the temperature of the approaching flow changes suddenly from 1000 to 600 K at $4000t'$ where an envelope flame has already developed. Regarding the other case, at the same time the surrounding temperature is down to a level of 400 K. The vaporization fluxes predicted by the quasi-steady models and by the transient solution for the two cases are plotted in Figures 11 and 12, respectively. In Figure 11, when the flow temperature changes, the predicted vaporization fluxes decrease immediately for all solutions. The transient solution reveals that, following the temperature decrease, the envelope flame can still be sustained around the droplet. It is also true for the upper-branch solution. As a consequence, the upper-branch solution and the combustion model coincide with the transient solution. On the other hand, because the pure vaporization state is obtained in the case of the lower-branch solution, it

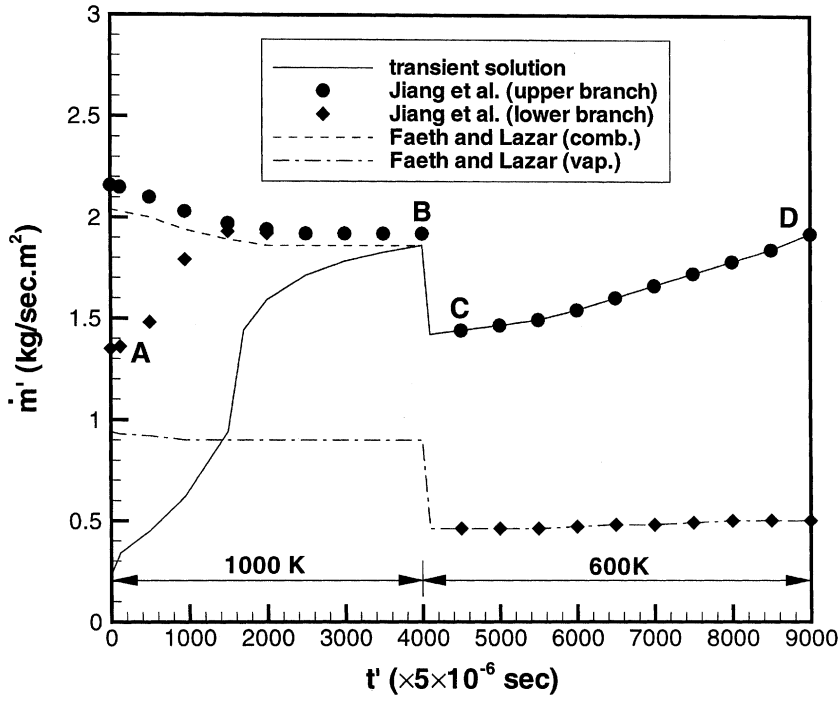

Figure 11. Comparison of droplet vaporization fluxes with respect to time (the ambient temperature suddenly drops from 1000 to 600 K at $4000t'$).

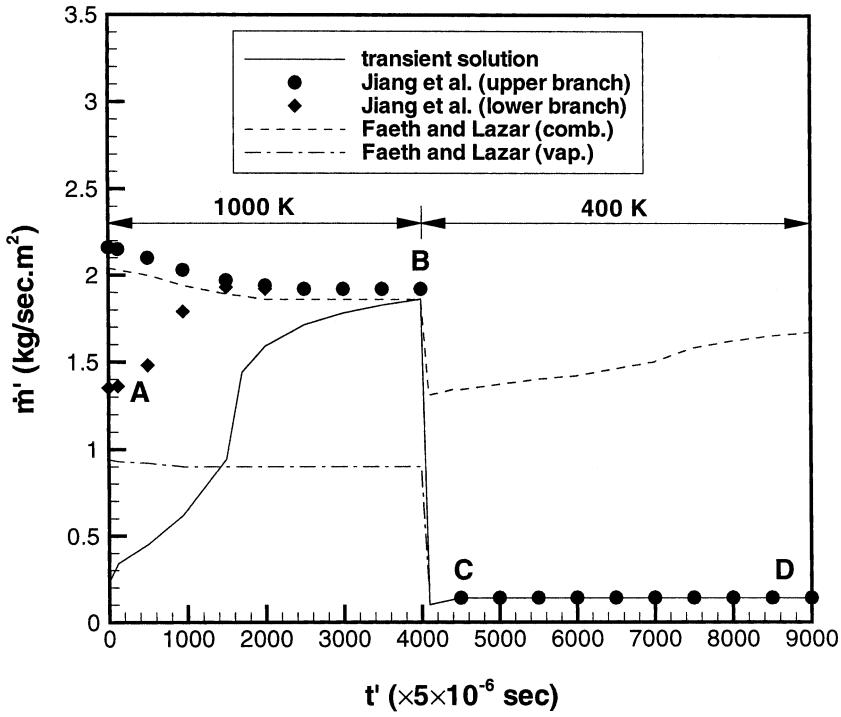

Figure 12. Comparison of droplet vaporization fluxes with respect to time (the ambient temperature suddenly drops from 1000 to 400 K at $4000t'$).

loses the application in estimating the vaporization flux. The same result is also found in the vaporization model of Faeth and Lazar. If the flow temperature is further reduced to 400 K, as seen in Figure 12, the transient solution indicates that the envelope flame no longer surrounds the droplet. The same result is also obtained by the lower- and upper-branch solutions. Therefore, excluding the combustion model of Faeth and Lazar, the vaporization fluxes evaluated by the quasi-steady models agree well with that of the transient solution. In summary, whatever the ambient temperature changes, the predicted vaporization flux in terms of the dual solution model will follow path A–B–C–D shown in Figures 11 and 12. From the preceding observations, it is realized that, when modeling a droplet in sprays, if the burning process that the droplet undergoes is regarded, the dual solution model is capable of providing a best prediction on droplet vaporization rate.

Influences of Droplet Size and Pressure

In Figure 13, the variations in mass flux under various droplet radii are evaluated while the case of a 100- μm-radius decane droplet is considered as well. In the figure the relative velocity between the droplet and the gas phase is fixed as 40 m/s, implying that the smaller the droplet, the smaller the droplet Reynolds number. Relative to the droplet of 100- μm-radius, when the droplet radius is 50 μm, despite the Reynolds number being reduced by a factor of 2, more energy from the interface can be used for vaporization rather than internal heating. Besides, it is conducive to the formation of the envelope flame (at $1800t'$). Consequently, the mass flux of the 50-μm-radius droplet is much higher than that of the other droplets. Contrary to the preceding result, for the case of 150 μm, more heat is required for heating the droplet while it is more difficult to established an envelop flame. This results in a lower mass flux distribution. Regarding the decane droplet, its boiling point and latent heat are

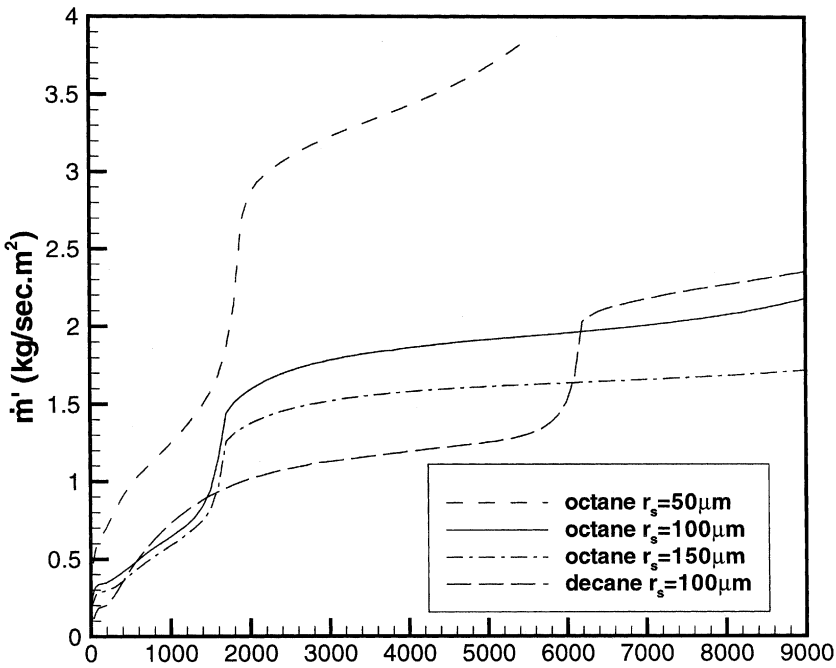

Figure 13. Comparison of droplet vaporization fluxes with respect to time under various droplet sizes and fuels ($u_{g\infty} = 40$ m/s and $p_{g\infty} = 1$ atm).

447.3 K and 66.8 kcal/kg, respectively, whereas they are 398 K and 72.5 kcal/kg for the octane droplet. In the early period, the time required for the decane droplet approaching the wet bulb temperature is longer; hence, its distribution in mass flux is lower than that of the octane droplet. However, once the envelope flame is exhibited around $6200t'$, because of the lower value of the latent heat, the distribution of the decane is higher. This further reflects that, in the initial period, the difference between the transient solution and the quasi-steady models shown in Figures 11 and 12 will be substantial. Eventually, the influence of the ambient pressure on the burning process of the octane droplet with 100-μm-radius is studied in Figure 14. Three different ambient pressures of 1, 3, and 5 atm are selected. The isothermal contours around the droplet at $t = 3000t'$ are plotted in the figure as well. Basically, when the ambient pressure is increased, the gaseous density will be increased, thereby

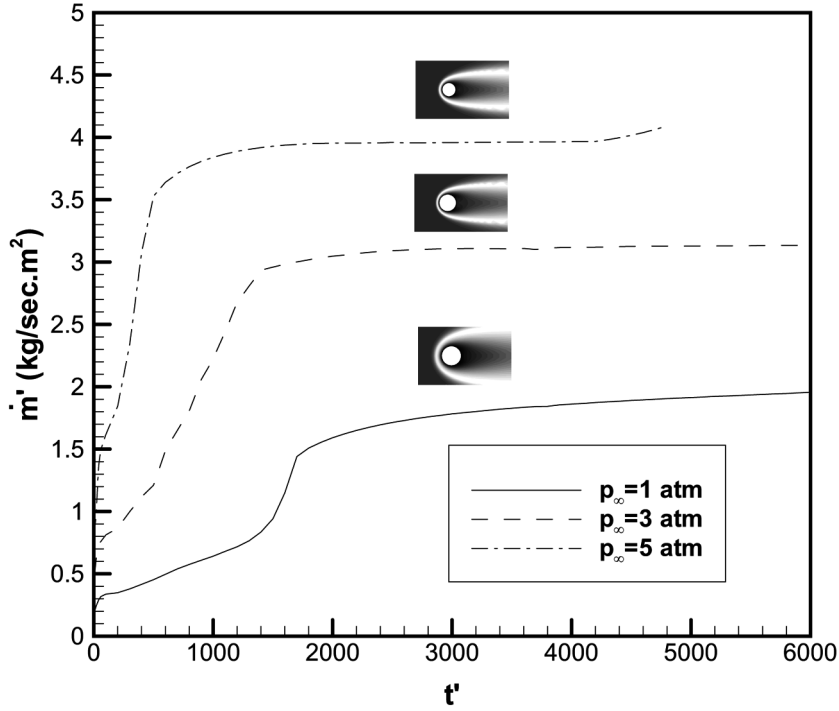

Figure 14. Comparison of octane droplet vaporization fluxes with respect to time at three different ambient pressures ($r_s = 100\,\mu m$ and $u_{g\infty} = 40\,m/s$).

enhancing the Damköhler number. As a result, as shown in Figure 14, increasing the ambient pressure increases the droplet mass flux, resulting from intensifying the fuel vapor combustion. It follows that the burning characteristics of a droplet are very sensitive to the surrounding pressure.

CONCLUSIONS

The transient burning process and internal heating of a convective droplet in flow have been investigated by using the fully numerical simulation method for both the gas- and droplet-phase flows. The flame configuration of a droplet, which is suddenly exposed to a hot stream, starts with pure vaporization, and then proceeds through a wake flame, a transition flame, and eventually to an envelope flame. Both the numerical simulation and theoretical analysis suggest that most of the time the droplet internal heating is dominated by the internal circulation. The droplet Reynolds number decreases with time because of drag force and vanishing droplet size, and the droplet vaporization flux increases monotonically throughout the entire droplet lifetime. The applications of the quasi-steady models have been examined as well. By virtue of greater temperature gradient in the initial droplet heat-up period, heat transfer from the ambience mainly contributes to heating the droplet interior rather than vaporization. As a result, all the quasi-steady models were found to be inadequate. However, as long as the envelope flame encloses the droplet, the predictions by the quasi-steady models, except for the vaporization model, are in good agreement with the transient solution. As a whole, because the envelope flame dominates the entire burning process, the droplet vaporization rate can be modeled well by the quasi-steady approximation, thereby significantly reducing computational time when performing spray-combustion simulation. Additionally, if the droplet experiences a sudden drop in the ambient temperature, the result elucidates that the dual solution model is still capable of providing a satisfactory prediction in droplet vaporization rate. Therefore, it is concluded that if one intends to utilize a quasi-steady model to evaluate the droplet behaviors in sprays, the droplet historical state should be considered. However, it is noteworthy that if a liquid droplet with higher boiling point such as decane is considered, the disagreement between the transient solution and the quasi-steady models may become substantial, resulting from the internal heating being more significant throughout the entire droplet lifetime.

NOMENCLATURE

B	Spalding transfer number
C_D	drag coefficient
C_p	specific heat of constant pressure
D	diffusivity
h	sensitive enthalpy
k	thermal conductivity
L	latent heat
N	number of species
$\dot{m}$	droplet vaporization rate
$\dot{m}'$	droplet vaporization flux
$\dot{m}_\theta$	droplet local vaporization flux
p	pressure
Pr	Prandtl number
Q	heat of combustion
r	radial coordinate
r_s	droplet radius
Re	Reynolds number
R_u	universal gas constant
Sc	Schmidt number
T	temperature
t	time
t'	convective time
u	axial velocity
v	radial velocity
W	molecular weight
x	axial coordinate
Y	mass fraction

Greek Symbols

α	thermal diffusivity
θ	polar angle
μ	viscosity
ν	kinematic viscosity
ρ	density
τ_{Hg}	gas hydrodynamic-diffusion time
$\dot{\omega}$	specific chemical reaction rate

Subscripts

0	initial state or stationary state
f	fuel or friction drag
g	gas phase
i	*i*th species
l	liquid phase
n	normal direction
o	oxidizer
p	pressure drag
ref	reference
s	droplet surface
t	thrust drag
θ	tangential direction
∞	upstream far field

REFERENCES

Chen, W.H. (2000a) Partially premixed flame structure and stability of twin droplets in flows. *J. Heat Transfer—Trans ASME*, **122**, 730.

Chen, W.H. (2000b) Combustion hysteresis and vaporization interaction of two burning droplets with different sizes. *Combust. Sci. Technol.*, **154**, 229.

Chen, W.H. (2002) Brachial burning and gasification split of a two-droplet system. *Atomiz. Sprays*, **12**, 29.

Chen, W.H., Liu, C.C., and Jiang, T.L. (1998) Hysteresis Effects of Two Interactive Droplets Burning in Convective Flows. *Proc. Combust. Instit.*, **27**, 1923.

Chiang, C.H., Raju, M.S., and Sirignano, W.A. (1992) Numerical analysis of convecting, vaporizing fuel droplet with variable properties. *Int. J. Heat Mass Transfer*, **35**, 1307.

Chiu, H.H. (2000) Advances and challenges in droplet and spray combustion. I. Toward a unified theory of droplet aerothermochemistry. *Prog. Energy Combust. Sci.*, **26**, 381.

Chiu, H.H. and Huang, J.S. (1996) Multiple-state phenomena and hysteresis of a combusting isolated droplet. *Atomiz. Sprays*, **6**, 1.

Chiu, H.H. and Hu, L.H. (1998) Dynamics of Ignition Transience and Gasification Partition of a Droplet, *Proc. Combust. Instit.*, **27**, 1889.

Dwyer, H.A. (1989) Calculations of droplet dynamics in high temperature environments. *Prog. Energy Combust. Sci.*, **14**, 131.

Faeth, G.M. (1977) Current status of droplet and liquid combustion. *Prog. Energy Combust. Sci.*, **3**, 191.

Faeth, G.M. and Lazar, R.S. (1971) Fuel droplet burning rates in a combustion gas environment. *AIAA J.*, **9**, 2165.

Glassman, I. (1996) *Combustion*, Academic Press, San Diego, CA.

Huang, J.S. and Chiu, H.H. (1997) Multistate behavior of a droplet in dilute sprays. *Atomiz. Sprays*, **7**, 479.

Jiang, T.L., Chen, W.H., Tsai, M.J., and Chiu, H.H. (1994) Double flame and multiple solution computations for a wetted porous sphere vaporizing in reactive flows. *Combust. Sci. Technol.*, **102**, 115.

Jiang, T.L., Chen, W.H., Tsai, M.J., and Chiu, H.H. (1995) A numerical investigation of multiple flame configurations in convective droplet gasification. *Combust. Flame*, **103**, 221.

Kuo, K.K. (1986) *Principles of Combustion*, John Wiley and Sons, New York.

Law, C.K. (1982) Recent advances in droplet vaporization and combustion. *Prog. Energy Combust. Sci.*, **8**, 171.

Law, C.K. (1984) Heat and mss transfer in combustion: Fundamental concepts and analytical techniques. *Prog. Energy Combust. Sci.*, **10**, 295.

Prakash, S. and Sirignano, W.A. (1978) Liquid fuel droplet heating with internal circulation. *Int. J. Heat Mass Transfer*, **21**, 885.

Prakash, S. and Sirignano, W.A. (1980) Theory of convective droplet vaporization with unsteady heat transfer in the circulating liquid phase. *Int. J. Heat Mass Transfer*, **23**, 253.

Patankar, S.V. (1980) *Numerical Heat Transfer and Fluid Flow*, Hemisphere, Washington, DC.

Patankar, S.V. (1981) A calculation procedure for two-dimensional elliptic situations. *Num. Heat Transfer*, **4**, 409.

Reid, R.C., Prausnitz, J.M., and Poiling, B.E. (1988) *The Properties of Gases and Liquids*, McGraw–Hill, New York.

Renksizbulut, M. and Haywood, R.J. (1988) Transient droplet evaporation with variable properties and internal circulation at intermediate Reynolds numbers. *Int. J. Multiphase Flow*, **14**, 189.

Sirignano, W.A. (1984) Fuel droplet vaporization and spray combustion theory. *Prog. Energy Combust. Sci.*, **9**, 291.

Sirignano, W.A. (1999) *Fluid Dynamics and Transport of Droplets and Sprays*, Cambridge University Press, Cambridge, MA.

Thompson, I.F., Warsi, Z.U.A., and Mastin, C.W. (1985) *Numerical Grid Generation*, North-Holland, New York.

Westbrook, C.K. and Dryer, F.L. (1981) Simplified reaction mechanisms for the oxidation of hydrocarbon fuel in flames. *Combust. Sci. Technol.*, **27**, 31.

Williams, F.A. (1985) *Combustion Theory*, 2nd ed., Benjamin-Cummins, Menlo Park, CA.

Wong, S.C. and Lin, A.C. (1992) Internal temperature distributions of droplets vaporizing in high-temperature convective flows. *J. Fluid Mech.*, **237**, 671.